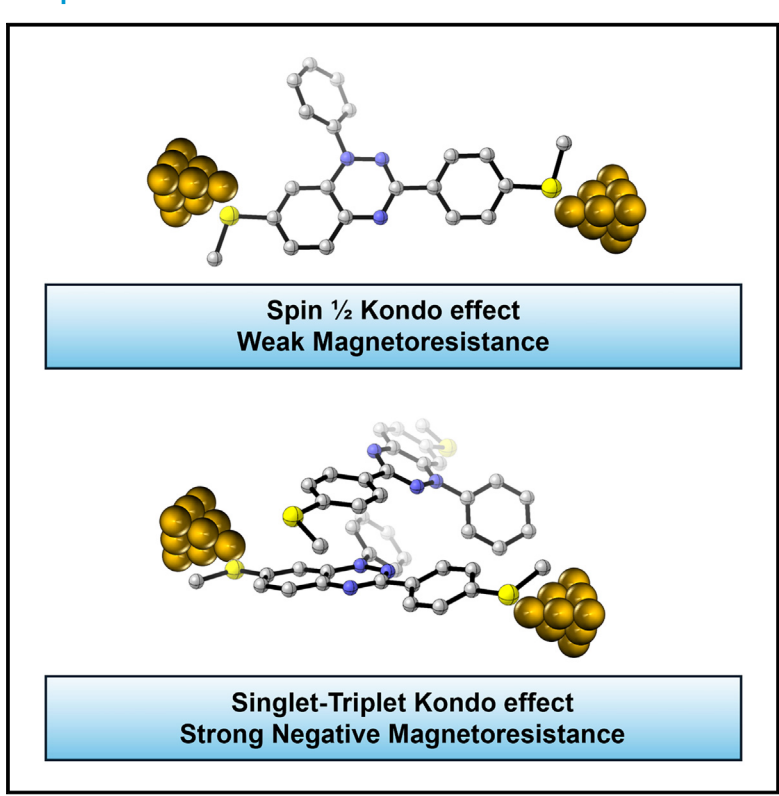
Chem

Conventional versus singlet-triplet Kondo effect in Blatter radical molecular junctions: Zero-bias anomalies and magnetoresistance

Graphical abstract



Highlights

- Blatter radical single-molecule junctions in a two-terminal device at low temperature
- Coexistence of Kondo effect and magnetoresistance in the same system
- High negative magnetoresistance due to the singlet-triplet Kondo effect

Authors

Gautam Mitra, Jueting Zheng, Karen Schaefer, ..., Carmen Herrmann, Theo A. Costi, Elke Scheer

Correspondence

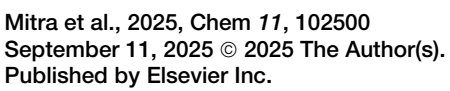
elke.scheer@uni-konstanz.de

In brief

We showcase the stability of Blatter radical single-molecule junctions in a two-terminal system at cryogenic conditions. Here, we characterize different types of Kondo effects and negative magnetoresistance originating from multiple configurations of the junctions. By combining break junction experiments and quantum-transport calculations, we reveal a detailed understanding of the correlation between different magnetotransport properties for the first time.











Chem



Article

Conventional versus singlet-triplet Kondo effect in Blatter radical molecular junctions: Zero-bias anomalies and magnetoresistance

Gautam Mitra,^{1,2} Jueting Zheng,^{1,3} Karen Schaefer,⁴ Michael Deffner,^{4,5} Jonathan Z. Low,⁶ Luis M. Campos,⁶ Carmen Herrmann,^{4,5} Theo A. Costi,⁷ and Elke Scheer^{1,8,*}

THE BIGGER PICTURE Spintronics is now a rapidly growing area of research that holds promise to transform the technological landscape of quantum information science. At the molecular level, understanding the behavior of stable radicals can lead to fundamental guidelines to control electron spin transport, especially in metal-molecule-metal junctions. To date, charge transport has played a significant role in molecular electronics, and turning toward single-electron open-shell molecules can lead to molecular systems for data storage and quantum-enabled devices.

Here, we report the behavior of the Blatter radical embedded in a magnetically controlled break junction, where the radical remains intact. We also found two different anomalies that we experimentally and theoretically characterized as different configurations within the junction, and importantly, these systems also exhibit a singlet-triplet Kondo effect. These findings are setting the foundation for investigating structure-property relationships of stable radicals and can lead to expanding the arsenal of building blocks for spintronics.

SUMMARY

The Blatter radical has been suggested as a building block in future molecular spintronic devices because of its radical character and expected long spin lifetime. However, whether its radical character is maintained in single-molecule junctions depends on the environment. Here, we demonstrate the ability to retain the open-shell nature of the Blatter radical in a two-terminal device by the appearance of a Kondo resonance in transport spectroscopy. Additionally, a high negative magnetoresistance is observed in junctions that do not reveal a zero-bias anomaly. By combining distance-dependent and magnetic-field-dependent measurements and accompanying quantum-chemical and quantum-transport calculations, we show that both findings, the negative magnetoresistance and the Kondo features, can be consistently explained by a singlet-triplet Kondo model. Our findings provide the possibility of using the Blatter radical in a two-terminal system under cryogenic conditions and also reveal the magnetotransport properties emerging from different configurations of the molecule inside a junction.

INTRODUCTION

Stable organic radical molecules are emerging to become key components for spin-based molecular electronic materials and devices.¹⁻⁶ They are open-shell systems that do not readily decompose or chemically react under standard conditions and whose stability can be engineered by virtue of chemical design.⁷⁻¹⁰ First reported in 1968,¹¹ the 1,2,4-benzotriazin-4-yl



¹Department of Physics, University of Konstanz, 78457 Konstanz, Germany

²Institute of Condensed Matter and Nanosciences, Université Catholique de Louvain (UCLouvain), 1348 Louvain-la-Neuve, Belgium

³State Key Laboratory of Physical Chemistry of Solid Surfaces, College of Chemistry and Chemical Engineering, Xiamen University, Xiamen 361005, China

⁴Department of Chemistry, University of Hamburg, 22761 Hamburg, Germany

⁵The Hamburg Centre for Ultrafast Imaging, 22761 Hamburg, Germany

⁶Department of Chemistry, Columbia University, New York, NY 10027, USA

⁷Peter Grünberg Institut, Forschungszentrum Jülich, 52425 Jülich, Germany

⁸Lead contact

^{*}Correspondence: elke.scheer@uni-konstanz.de https://doi.org/10.1016/j.chempr.2025.102500





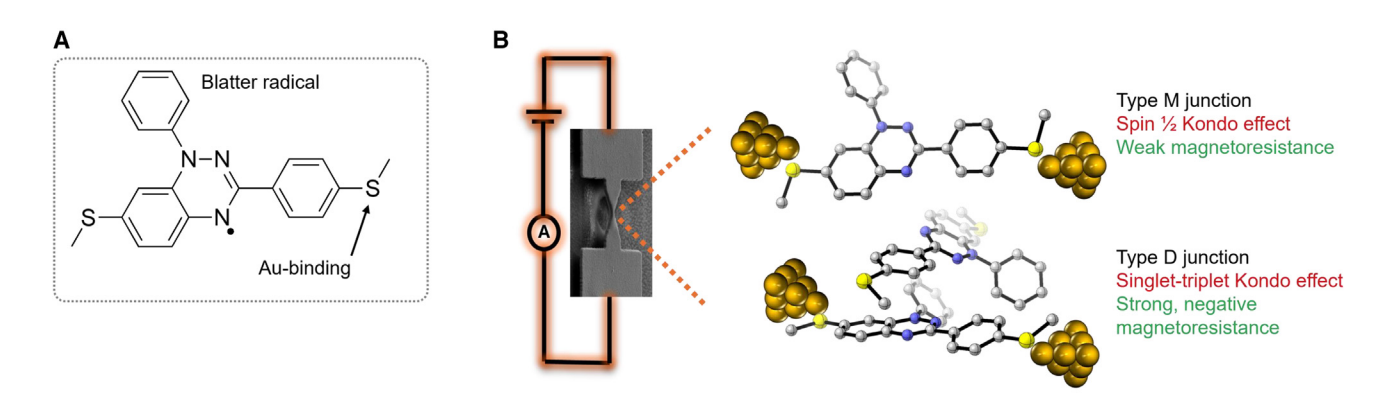


Figure 1. Illustration of the Blatter radical molecular junctions

(A) The chemical structure of the Blatter radical molecule used in this study.

(B) Schematic of the types of Blatter radical molecule junctions formed between two Au electrodes on an MCBJ device. Type M indicates a monomer junction, and type D indicates a dimer junction.

radical, commonly known as the Blatter radical, is one of such species and has gained interest because of its many exciting physical and chemical properties. ^{12–14} The stability of the Blatter radical under various circumstances enables it to be incorporated into manifold electronic devices, ^{15–17} including photodetectors ¹⁸ and thermoelectric devices. ¹⁹ In addition, the presence of an unpaired electron in this molecule can lead to interesting magnetic properties when interfaced with metallic substrates and electrodes. ^{16,17,20,21}

Blatter radicals typically have the unpaired electron delocalized on the molecule (Figure 1A). This spatial delocalization of the unpaired electron gives rise to the exceptionally high stability of the radical. Recently, these systems have been subject to studies under different environments of metal-molecule interfaces and have been shown to retain the open-shell nature in thin films¹⁵ and upon adsorption on the Au(111) surface under high vacuum. 16 Typically, Kondo spectroscopy is used as evidence for interrogating the molecular spin of the radical. 22,23 Previously, using scanning tunneling microscopy (STM) techniques under ultrahigh vacuum conditions, Repp and coworkers revealed a Kondo resonance arising from the interaction between the unpaired electron of the Blatter radical with the conduction electrons. 17 The singly occupied molecular orbital (SOMO) of the Blatter radical lies close to the Fermi level of Au and was suggested to be very sensitive to the environment around the molecule. 16 Little emphasis has been given to the study of Blatter junctions in a two-terminal metal-molecule-metal system, mainly because of the suspected loss of the open-shell character upon oxidation, as reported in solution-based STM-break junction experiments. 16 Later studies showed that functionalizing the radical by adding an electron-withdrawing group lowers the energy levels inside the molecule, giving more stability and preventing oxidation.¹⁹ Recently, Jiang et al. also explored this problem theoretically by using first-principle quantum-transport calculations.²⁴ Their calculations suggest that the Blatter radical can successfully retain its open-shell character in a junction between Au electrodes irrespective of the environmental conditions since the dative bonding at the molecule electrode interface does not alter the spin states of the radical.

We posit that stable organic radical junctions can also manifest unconventional magnetotransport behavior in combination with spectroscopic evidence for the Kondo effect and that both can be tuned by the coupling strength to the electrodes. To the best of our knowledge, no experimental magnetoresistance (MR) studies to date have focused on radicals with a delocalized unpaired electron in the current pathway by using in situ tunable yet sufficiently stable electrodes. To better understand the intrinsic properties of open-shell systems, here, we carried out the first systematic transport study of the Blatter radical in a mechanically controlled break junction (MCBJ) operated at low temperature. We were able to produce Blatter molecule junctions with increased stability in a two-terminal device and confirmed the signature of the open-shell nature of the radical by dI/dV spectroscopy. We synthesized the Blatter radical with two methylthioether units (-SCH₃) to enable coupling with the Au electrodes. 16 We deposited the molecule by using a dropcasting technique and carried out the electronic transport measurements of the individual junctions in cryogenic vacuum at a temperature of 4.2 K and under magnetic fields. Kondo resonances and magnetoresistance (MR) originating from stable organic radical molecule junctions have been studied with the MCBJ technique before. 16,25-27 However, in all previous cases, the electronic lone pair was located in a specific site of the molecule and was sterically protected. We have found two types of Kondo resonances, presumably originating from different configurations of the individual junctions of the Blatter radical molecule. One type of the observed Kondo resonances features a Kondo temperature (T_K) of 30–35 K with a broad and asymmetric line shape, and the other type has a $T_{\rm K}$ of 11-17 K with a more symmetric and narrow line shape. We confirmed the Kondo nature with the evolution of the zero-bias peak as a function of the magnetic field. These exhibit only a very weak negative finitebias MR, as predicted by the usual Kondo effect at finite bias (see Figure S1). However, we also observed a significant negative finite-bias MR in certain junctions without having a zerobias peak at the measurement temperature of 4.2 K. We found a maximum change of 21% in resistance with an applied magnetic field of ±8 T and a subsequent saturation of MR for higher





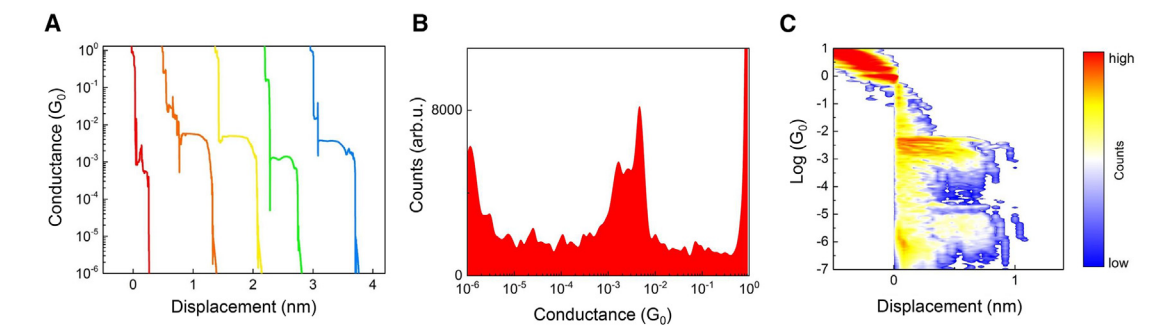


Figure 2. Conductance traces and histograms of Blatter radical at low temperature

- (A) Examples of typical opening traces of Blatter radical molecule junctions using the MCBJ method at 4.2 K.
- (B) 1D conductance histogram built from 595 opening traces measured at 4.2 K with 100 mV bias.
- (C) Two-dimensional histogram calculated from the same data as shown in (B).

fields. These results highlight the stability of the unpaired electron in the Blatter radical molecule junctions in low-temperature measurements with an MCBJ device. Finally, the negative MR at finite bias is explained in the framework of a singlet-triplet Kondo model. We have illustrated that the presence of an extra side-coupled molecule in the Blatter junction with an antiferromagnetic exchange interaction between the unpaired spins on the two radicals results in a possible scenario of negative MR at finite-bias voltage and at a temperature similar to the experiment. A summary of our results from different types of junctions is schematically shown in Figure 1B.

RESULTS

Statistical investigations

The Blatter radical molecule with two methylthioether units was synthesized and characterized as reported earlier. ¹⁶ The freshly prepared solution of the molecule was prepared in tetrahydrofuran (THF) and dropcast onto a gold (Au) MCBJ sample at room temperature in a nitrogen atmosphere and properly dried for 45 min. The sample was then characterized with a dipstick equipped with an MCBJ mechanism pumped to high vacuum and cooled down to 4.2 K inside a liquid-He bath cryostat. More details of sample preparation and measurement techniques are described in the methods section.

First, we measured and analyzed the opening traces of the Blatter radical molecule with an applied bias of 100 mV at 4.2 K. Figure 2A shows typical examples of these opening traces as a function of electrode displacement. Au singleatom contacts with $1G_0$ are observed in all the opening curves, where $G_0 = 2e^2/h$ is the conductance quantum. Below $1G_0$, upon further stretching of the electrodes, conductance plateaus are formed corresponding to the single-molecule junctions of the Blatter radical molecule bridged using methylthioether anchoring units. These plateaus show a maximum displacement up to 0.6 nm before breaking down to the tunneling regime, with conductance G below $10^{-6}G_0$. In Figure 2B, we constructed a conductance histogram with logarithmic binning of 595 opening traces without any data selection. We observed major conductance peaks between 10⁻² and 10^{-3} G_0 . We attribute multiple peaks observed in this conductance range to different configurations of molecular junctions formed between the Au electrodes. Flat plateaus observed in the opening traces correspond to fully stretched junctions of individual molecules, while partially connected junctions show fluctuations in conductance as the electrode displacement is increased. This behavior is also clearly apparent in the twodimensional conductance-distance histogram shown in Figure 2C. In addition to single-molecule junctions consisting of one molecule bridging the electrodes (denoted as monomer or M junctions), there is also the possibility of dimer (or D) junctions with two parallel or side-coupled molecules. To substantiate this possibility, we performed quantum-chemical calculations using density functional theory (DFT), see Method S4, the main results of which can be summarized as follows: first, the Blatter radicals investigated here have an affinity to each other, as reported earlier for similar species.^{2,28} Second, the simulated zero-bias conductance values are in the range of 10^{-2} to $10^{-3}G_0$ with the M junctions at the lower end of this range (in line with²⁴), and the higher ones corresponding most likely to D junctions. The thioether linkage is known to exhibit slight binding variations, which can arise from the rotation between the aryl group and -SMe.²⁹ Here, we attribute the difference in conductance values to the probability of junction formation of a given conformer. Also, the DFT calculations reported in the supplemental information show that there are several junction geometries with slightly different conductance values (the absolute conductance values are usually overestimated in DFT models). Regarding the junctions bearing two molecules, i.e., dimer (D) junctions, we stress that the differences are not due to the conformations but rather to different types of interactions between two molecules in the junction. Among the many possible D junctions, we find two particular configurations that are most stable. These are, at first, dimers where one Blatter radical is bridging between the electrodes, and the second one is connected with one of its thioether groups to one of the electrodes. The second type is formed by one Blatter radical bridging between the electrodes, while the second one π -stacks to the first but does not connect to the electrodes (see Method S4 for visuals). Knowing that DFT has the tendency to overestimate the conductance, 30-33 it appears likely that D junctions are also realized in the experiments.





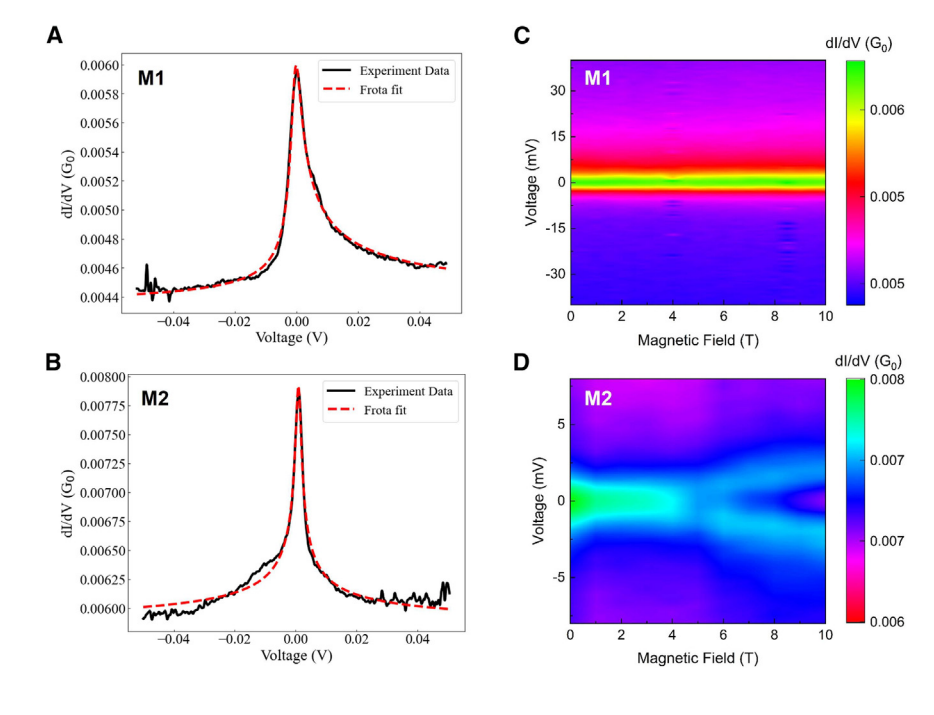


Figure 3. dI/dV analysis of different single-molecule junctions of the Blatter radical

(A) dI/dV spectra of a type M1 junction showing a broad zero-bias anomaly and fitted using the Frota function.

(B) Spectra of a type M2 junction showing a narrow zero-bias anomaly and fitted using the Frota function.

(C) Magnetic field dependence of the *dl/dV* spectra shown in (A) from 0-10 T at 4.2 K. No splitting of the zero-bias peak is observed here until 10 T

(D) Magnetic field dependence of the *dl/dV* spectra shown in (B) from 0–10 T at 4.2 K. A splitting of the zero-bias peak is observed approximately around 7 T.

This interpretation is in line with the relatively strong binding between the radicals. We will come back to this aspect further below. Finally, we note the possibility of π -stacked junctions, where the two radical molecules are connected to different electrodes each. These junctions are expected to have much lower conductance³⁴ and might give rise to the faint maxima around 10^{-4} to $10^{-5}G_0$ in the histograms.

The observed conductance peak in the histogram is also in close agreement with the previous studies of the same molecule on a solution-based scanning electron microscopy break junction (STM-BJ) experiment ¹⁶ and STM studies on thin films of the Blatter radical on a Au surface at room temperature. ¹⁷ Jiang et al. very recently tackled the small conductance obtained from the Blatter radical molecule junctions theoretically by using first-principle quantum-transport calculations. ²⁴ They attribute their unexpectedly low conductance to singly occupied frontier orbitals (SOMO and SUMO, respectively) being weakly electronically coupled to the Au electrodes. Hence, the Blatter radical may retain its unpaired spin upon contacting with Au electrodes in more instances than previously thought. In order to verify this hypothesis, we carried out several magnetotransport measurements on individual junctions as explained below.

Transport spectroscopy in individual junctions: Kondo resonances

Differential conductance spectroscopy is performed in order to understand the properties of individual Blatter radical molecule junctions in detail. We discuss the dl/dV characteristics observed in different junctions, which are measured using a lock-in amplifier technique with 0.1 mV AC amplitude. These measurements reveal a clear zero-bias anomaly indicating an electronic resonance formed near the Fermi level for about 20% of single-molecule junctions measured in our study. We have observed that the line width and the line shape of this reso-

nance vary among different junctions under the same measurement conditions. Figures 3A and 3B show examples of two junctions exhibiting different *dl/dV* spectra. Junction M1 (3A) shows a broad and asymmetric line shape, and junction M2 (3B) shows a narrower and symmetric

resonance. We attribute the origin of these zero-bias anomalies to Kondo resonances due to the presence of an unpaired electron in the current pathway, hence indicating that the open-shell radical nature of the molecule within the two-terminal device is maintained at low temperature. Furthermore, we argue that these junctions are monomer junctions, as we will discuss below.

For the junction M1, in Figure 3A, the zero-bias peak resembles a Fano resonance line shape as observed in many previous mesoscopic and nanoelectronics devices at low temperature.^{22,35} This type of spectrum was also previously reported with STM-based studies of the Blatter radical molecule. 16,17 A Fano line shape typically occurs when there is an interference between resonant transport channels and non-resonant direct tunneling pathways through the device under study. 36,37 Here, these are the transport assisted through the SOMO due to an unpaired spin, interfering with the continuum tunneling channels. The first pathway is responsible for the Kondo resonance, while the latter corresponds to the broad conductance background. This is often described by a Fano lineshape of the form $dI/dV \sim (q+\epsilon)^2/(1+\epsilon^2)$, with $\epsilon = (eV - E_K)/\Gamma_K$. The Fano parameter, q, defines the ratio of transmission amplitudes through the resonant and non-resonant tunneling channels and hence the peak asymmetry. Within this approach, the Kondo resonance is assumed to be a Lorentzian at energy EK with halfwidth Γ_{K} . However, numerical renormalization group (NRG) calculations show that the Kondo resonance has a non-Lorentzian lineshape with logarithmic tails decaying as $1/\ln^2(|eV|/k_BT_K)$ at $|eV| \gg k_BT_K$.³⁸ The Frota function,³⁹ which interpolates the low-temperature NRG spectra in the experimentally relevant range $|eV| < 10k_BT_K$, approximately captures this non-Lorentzian lineshape. Including the Fano effect within a Frota function description of the Kondo resonance yields for $dI/dV^{39,40}$

Chem Article



$$dI/dV = b - c \operatorname{Im} \left[i e^{i\phi} \sqrt{\frac{i\Gamma_{\rm F}}{E - E_{\rm K} + i\Gamma_{\rm F}}} \right],$$
 (Equation 1)

where $\Gamma_{\rm F}=\Gamma_{\rm K}/2.542$ and $\varphi=\varphi(q)$ are related to the Fano parameter q (see supplemental information and Figure S11) and constants b and c describe the background and Kondo peak amplitude, respectively. Equation 1 holds at low-temperature $T\ll T_{\rm K}$, where $\Gamma_{\rm K}$ acquires its zero-temperature value. This assumption holds in this experiment (as verified a posteriori by our fits to Equation 1). A comparison between the Lorentzian (Fano)- and Frota-based procedures is given in the Figure S3 and Table S1 lists all parameters extracted from fitting junctions M1 and M2 to Equation 1.

For the junction shown in Figure 3A, we find the energy width $\Gamma_{\rm K}$ = 4.5 mV. We can extract the Kondo temperature by using the result $k_{\rm B}T_{\rm K}$ = $2\Gamma_{\rm K}/\pi$, 41 and find it to be approximately 34 K. This is in good agreement with the values obtained in previous STM-based studies. 17 For junction M2, with $\Gamma_{\rm K}$ = 2.2 mV, we find $T_{\rm K}$ to be approximately 17 K.

The Kondo conductance and the lineshape depends on the strength of the coupling between the molecule and the electrodes and thus on the bonding sites of the molecule with the electrodes. 42,43 Hence, we argue that the resonances in cases M1 and M2 originate from different configurations of the molecular junction. Since we observed both flat and slanted opening traces in our study, the formation of single-molecule junctions with different configurations giving rise to different T_K is a likely scenario. For Blatter radicals, it is known that the spin density is mostly centered around the fused benzene ring, benzotriazinyl core and is partially delocalized to one of the phenyl rings attached with the thiomethyl groups. 17,21 The third aromatic ring is spin-isolated. Hence, the difference in electronic coupling with both ends of the electrodes can lead to varying coupling strengths and transport pathways. Consequently, the junctions with metal electrodes having a direct interaction with one of the higher-spin-density sites can display strong zero-bias resonances. Since the Fano line shape results from interference with another transport path, it is possible that M1 junctions arise from configurations where the open-shell radical interacts alone with the electrode. We analyzed many individual junctions with conductance values between 10⁻² and 10⁻³G₀ but found no clear correlation with $T_{\rm K}$ and G, whereas 70% of them show asymmetric resonance with a $T_{\rm K}$ of more than 30 K (type M1). An indepth theoretical calculation is necessary to distinguish between different Kondo states and junction structures.

To further validate the presence of the Kondo resonance and the extracted $\Gamma_{\rm K}$ (and $T_{\rm K}=2\Gamma_{\rm K}/\pi k_{\rm B}$) in these junctions, we recorded the evolution of dl/dV spectra at various magnetic fields from 0 to 10 T at 4.2 K. A magnetic field typically splits the Kondo resonance due to the Zeeman effect. Figures 3C and 3D show the corresponding spectra for junction M1 and junction M2, respectively. We observed no splitting or suppression of the zero-bias peak in junction M1 while a clear splitting of the peak is visible for junction M2. Theoretical predictions suggest that this splitting follows the relation $g\mu_{\rm B}B_{\rm c}\approx\Gamma_{\rm K}/2$. 44,45 For the junction M2, the splitting appears around the field $B_{\rm c}$ of \approx 7 T compared with the theoretical prediction 9.9 T using the ex-

tracted $\Gamma_{\rm K}=2.29$ mV. We did not observe any changes with increasing magnetic field up to the maximum experimentally accessible field of 10 T for junction M1. This is in agreement with the estimation from theory (using the extracted $\Gamma_{\rm K}=4.57$ mV) suggesting that the splitting is expected to occur only after ≈ 20 T, which is above our experimental limit. We thus infer that these junctions are similar to those reported earlier in Patera et al. 17 that were identified as Kondo junctions. Further examples for the evolution of dl/dV spectra under magnetic field for both types of junctions is given in the Figure S4. We found that the experimental field dependence of the dl/dV for all the measured junctions shows a remarkable agreement with the theoretical predictions, 44,45 showing a splitting close to the predicted B_c when this lies in the experimentally accessible field range and no splitting when B_c is predicted to lie outside this range.

Negative magnetoresistance and singlet-triplet Kondo effect

It was reported earlier that for single-radical molecular junctions without showing any Kondo features, a very pronounced MR can be observed at larger bias. MR is defined here as the relative change in resistance of a molecule junction at an applied magnetic field with respect to zero field. In order to study the magnetotransport on molecular junctions, which do not show any zero-bias peak in our measurements (denoted as type D junctions), we studied the evolution of the resistance under magnetic field applied perpendicular to the sample plane from -10 to 10 T (red) and 10 to -10 T (black) at a rate of 50 mT/min and measured with a constant bias voltage of 30 mV at 4.2 K. Figure 4 shows MR curves obtained from three such type D junctions.

We observed a strong negative MR (i.e., decrease of resistance with increasing field strength) with a maximum change of $\approx\!21\%$. Besides a small hysteresis, we observed no clear change in MR amplitude with the sweep direction. MR curves tend to saturate after approximately ± 8 T. We note that in previous studies of radical molecule junctions, this kind of saturation or maxima/minima of the resistance were also observed, but at different field value. We also found that all measured Blatter radical single-molecule junctions show exclusively negative MR in our study. In addition, MR measured on type M1 or M2 junctions show only a very small change in resistance of less than 2%, as given in the Figure S1, hence revealing an anti-correlation between Kondo behavior and strong MR. This behavior was first explored in junctions of the perchlortrityl radical molecule 46 and is now confirmed for Blatter junctions.

The origin and mechanism of large MR in molecule junctions are still under debate. Various mechanisms have been reported based on the studies of different organic radical molecules with regard to the exact structure of the molecule and anchoring groups. Most of these mechanisms rely heavily on the influence of molecule-electrode interface scattering and changes in the electronic coupling strength. ^{26,47,48} In our study, we used methylthioether anchoring units to couple the Blatter radical to the Au electrodes. The previous study on the perchlortrityl radical molecule using the same anchoring groups yielded both positive and negative MR that was assigned to spin-dependent scattering at the molecule-electrode interfaces and resulting in a quantum





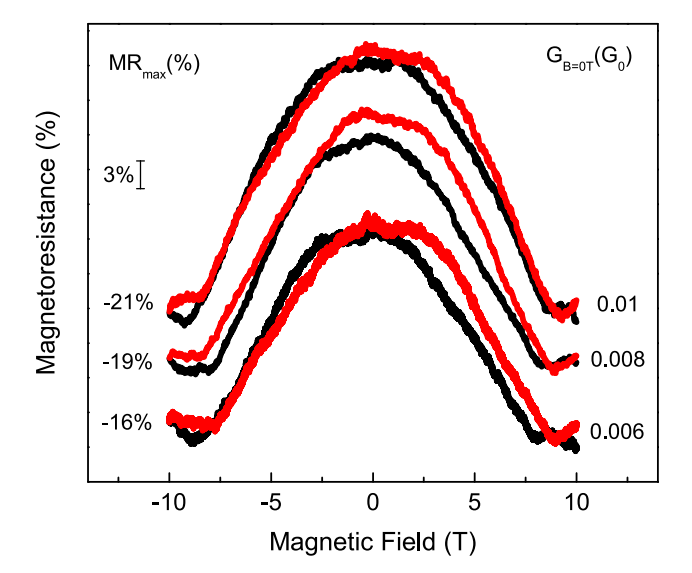


Figure 4. Magnetoresistance measurements of Blatter radical junctions without a zero-bias anomaly (type D junctions) at different conductances

The magnetic field is swept from $-10\,\text{T}$ to $10\,\text{T}$ and back with a sweep rate of 50 mT/min at 4.2 K, and the resistance is measured with an applied bias of 30 mV. The maximum MR% observed is indicated for each junction. Black curves represent a magnetic field sweep direction from $10\,\text{T}$ to $-10\,\text{T}$ and red curves from $-10\,\text{T}$ to $10\,\text{T}$. MR scale bar corresponds to 3% as indicated.

interference effect.⁴⁶ In the case of Blatter molecule junctions, we observed exclusively negative MR, and the theoretically reported weak electronic coupling of SOMO and SUMO orbitals with gold electrodes suggests the above MR mechanisms may not be prominent.

Hence, we propose a possible explanation of the significant negative MR of type D junctions, assuming the junctions actually consist of a double quantum dot system: a Blatter molecule in the junction side-coupled to a second quantum dot, also having a S = 1/2, resulting in an antiferromagnetic exchange interaction of strength J between the two (see Equation 2 in theoretical methods and the Method S2). The second quantum dot could be, e.g., a gold atom or a cluster with unpaired spin, a molecular fragment, or a second Blatter radical. As mentioned above, the existence of structures in which a second Blatter radical couples with the first is supported by our quantum-chemical calculations (see Method S4). Furthermore, we found most such pairs to preferentially couple antiferromagnetically, with a coupling constant J' (for a Hamiltonian of the form $H = -2J'S_aS_b$) in the range of around -90 to -140 cm⁻¹, which translates in our Kondo dimer model notation to antiferromagnetic couplings J = -2J' of order 20-40 meV, i.e., 200-400 K. Examples of the optimized structures of the possible dimer (D) junctions, the resulting transmission functions and the information about energies and spin population are given in the Method S4. Weak ferromagnetic coupling could also occur for some junctions based on our DFT calculations but could be pushed to more antiferromagnetic by binding to the electrodes. The latter possibility is also interesting as the D system would form a S=1, which would result in an underscreened Kondo effect.49

For antiferromagnetic couplings J, the double-dot system would exhibit the so-called singlet-triplet Kondo effect, which would provide a mechanism for understanding the observed negative MR in the absence of a zero-bias peak in dl/dV. Organic radical dimers, exhibiting a field-induced singlet-triplet Kondo effect have been investigated previously, however, the MR was not discussed.⁵⁰ Within this picture, see Figure 5A, the ground state of the isolated dimer at B = 0 is a singlet S = 0 state with a triplet S = 1 state lying at an energy J above it. Upon coupling the dimer to the leads, the Kondo effect at low energies, temperatures, and voltages $(E, k_BT, eV \ll J)$ is therefore suppressed and a zerobias peak in dI/dV is absent for |eV| < J. Instead, the differential conductance exhibits a gap of order 2J, which at high temperatures $k_BT > J$ could be smeared out (see Figure S8A). Despite the non-magnetic ground state, the system is still strongly affected by a magnetic field via the effect of the latter on the polarizable triplet state: the magnetic field splits the triplet state and decreases the splitting $\delta(B) = E_{S=1,|S_z|=1} - E_{S=0,S_z=0}$ between the lowest component of the triplet state ($S_z = +1$ for B > 0or $S_7 = -1$ for B < 0) and the singlet state as shown in Figure 5A. This splitting eventually vanishes at a sufficiently large magnetic field $B = B^*$ where B^* is of the order of $J/g\mu_B$ ($B^* = J/g\mu_B$ exactly when the molecule plus side-coupled quantum dot is detached from the leads but is slightly reduced when it is attached to the leads⁵⁰). Fluctuations between the degenerate states at B =B* lead to a fully developed singlet-triplet Kondo effect via the hybridization of these states to the leads.⁵¹ In this scenario, increasing B from zero toward B^* induces the singlettriplet Kondo effect and thereby enhances the conductance G(B) = dI/dV, implying that G(B = 0) - G(B) is negative (i.e., positive magnetoconductance), resulting in a negative MR for the field range $-J < g\mu_B B < +J$ (see Figure 5B and S10). This is opposite to the usual S = 1/2 Kondo effect where a magnetic field reduces the conductance (resulting in a positive MR, see Figure S10).

Figure 5B shows the NRG calculations of the MR at several dimensionless voltages eV/k_BT_K for $J/k_BT_K = 100$. For all voltages, the MR is negative and exhibits a similar dependence on the magnetic field as in the experiment. It is largest at V = 0. Finite Vintroduces decoherence, leading to a suppression of the MR. Nevertheless, even at $eV/k_BT_K = 30$, the MR reaches 10% at $g\mu_B B/k_B T_K = 10$. The magnitude of the MR is sensitive to the precise J/k_BT_K and T/T_K (see Figure S9 for $J/k_BT_K = 30$ and $T/T_K = 10$). The effect of a longitudinal or transverse spin-exchange anisotropy $(J_{\parallel}/J_{\perp}=2 \text{ and } J_{\parallel}/J_{\perp}=1/2, \text{ respectively})$ is shown for the largest bias voltage ($eV/k_BT_K = 30$) and found to be small. Its effect is even smaller for smaller bias voltages (see supplemental information). In general, for |eV| < J, its effect is to enhance the magnitude of the MR, but its sign remains negative. Similarly, the effect of the Dzyaloshinskii-Moriya (DM) interaction enhances the magnitude of the MR, as shown in Figure 5 for two bias voltages (dotted lines) and a large D/J = 0.5. Importantly, the DM interaction does not affect its overall B-dependence or the negative sign of the MR (for smaller D/J = 0.2, the enhancement is much smaller, see Figure S9A). The enhancement in the magnitude of MR $\approx 1 - G(V, 0)/G(V, B)$ is due to the reduction of G(V, B)in the presence of a finite Dzyaloshinskii vector (D), relative to its value for D = 0 (since, a finite D enhances the pseudo-magnetic





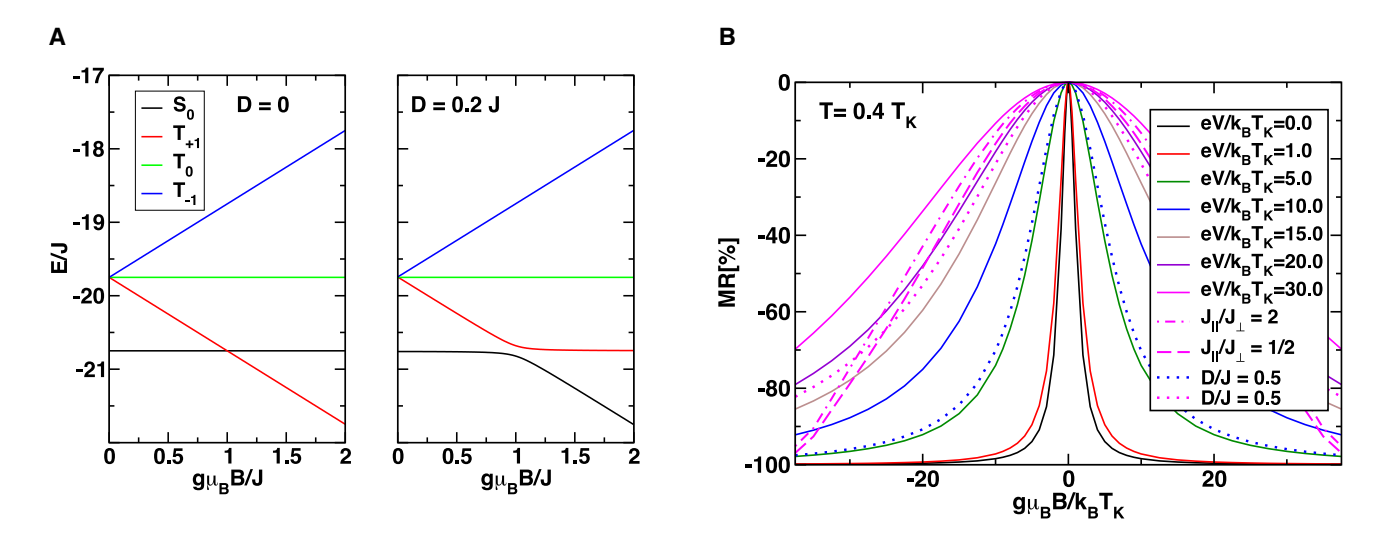


Figure 5. Singlet-triplet Kondo effect and negative magnetoresistance

(A) Magnetic field dependence of the lowest energy singlet (black, S_0) and triplet states (T_{+1} , T_{-1} , T_0) of a quantum dot with level energy $\epsilon_0 = -20J$ exchange coupled to a second S = 1/2 quantum dot with antiferromagnetic coupling with J = 10 meV, in the absence and in the presence of a Dzyaloshinskii-Moriya (DM) interaction, $H_D = D \cdot s_d \times S$.

(B) Magnetoresistance at temperature $T=0.4T_{\rm K}=4$ K for different values of the bias voltage $eV/k_{\rm B}T_{\rm K}=0$, 1, ..., 30 corresponding (approximately) to V=0, 1, ..., 30 mV and isotropic exchange $J/k_{\rm B}T_{\rm K}=100$ (solid lines). The effect of anisotropic spin exchange is also shown for the largest voltage V=30 mV: isotropic case $J_{\parallel}/J_{\perp}=1$ (magenta solid line), longitudinal anisotropy $J_{\parallel}/J_{\perp}=2$ with $J_{\parallel}/k_{\rm B}T_{\rm K}=100$ (magenta dashed-dotted line), and transverse anisotropy $J_{\parallel}/J_{\perp}=1/2$ with $J_{\perp}/k_{\rm B}T_{\rm K}=100$ (magenta dashed line). For completeness, although most likely not relevant for molecules solely composed of light atoms (e.g., the Blatter radical), we also show the effect of the Dzyaloshinskii-Moriya (DM) interaction. In order to discern the trends, this is shown for an unusually large D/J=0.5 for both V=10 mV and V=30 mV (dotted lines).

field $\delta(B)/g\mu_B$ in the singlet-triplet Kondo effect, thereby reducing G as discussed in 50). The intrinsically negative MR seen for dimer systems is in stark contrast to the positive (low bias) MR of a single Kondo-correlated quantum dot described by the Anderson impurity model in Figure S10, which is also in clear agreement with the previously reported studies. 46

DISCUSSION

We have developed single-molecule junctions of the Blatter radical molecule using a mechanically controlled break junction setup at low temperature in a cryogenic vacuum environment. Our detailed magnetotransport measurements suggest that the open-shell nature of the Blatter junction remains intact in a two-terminal junction. Differential conductance spectroscopy studies on individual contacts reveal two different types of zero-bias anomalies originating from the different configurations of the metal-molecule-metal junction. They are attributed to a Kondo resonance arising from the delocalized unpaired electron orbital situated in the current pathway. In addition, Blatter radical molecular junctions without a zero-bias peak showed strong negative MR with a maximum change of 21% in resistance measured at high bias voltage. We modeled the origin of these high negative MR toward junctions involving a Blatter molecule with strong correlation with a side-coupled quantum dot configuration, which results in a singlet-triplet Kondo effect. The detailed quantum-chemical calculations show qualitative agreement between the experiment and theoretical predictions. Our findings reconcile earlier, seemingly contradictory findings on Blatter radical molecular junctions studied in different environments and will open up several experimental and theoretical avenues to revisit the transport and magnetotransport properties of other radical molecular junctions. They also pave the way for studying various fundamental aspects of the Blatter radical and its derivatives to tailor their properties for spintronic applications.

METHODS

Device fabrication

The break junction devices were fabricated on a 500 µm thick, polished insulating Cirlex (Kapton laminate) substrate. 2 µm polyimide sacrificial layer was spin-coated on the substrate, baked at 130°C for 5 min, then hard-baked at 430°C for 90 min under vacuum. Next, a double-layer resist consisting of methylmethacrylat-methacrylic acid/polymethylmethacrylate (MMA-MAA/ PMMA) is spin-coated on top and baked in an oven at 170°C for 30 min. Electron beam lithography was performed on these substrates of size 3 × 18 mm² in a Zeiss Cross Beam machine at 10 kV acceleration voltage and was developed using 1:3 methyl isobutylketon: isopropylalcohol (MIBK:IPA) solution for 30 s and rinsed with pure IPA. 80 nm of Au were later deposited using the electron beam evaporation. The samples were then etched using anisotropic reactive ion etching in a mixture of oxygen and sulfur hexafluoride at 1 mbar with a power of 50 W for 30 min. This process removes about 600 nm of the polyimide layer below the electrodes. We prepared a 0.2 mM solution of Blatter molecules in tetrahydrofuran (THF) and then dropcast it





onto a freshly prepared MCBJ substrate in nitrogen atmosphere at room temperature and dried for ≈ 1 h.

Transport measurements

All experimental measurements were carried out using a custom-made cryogenic vacuum dipstick equipped with an MCBJ at 4.2 K in a He bath cryostat. The sample is shielded using a copper cap to prevent stray electromagnetic fields. The electrode displacement, δd , is calibrated by analyzing the opening curves of a bare Au break junction using the tunneling conductance expression $G(\delta d) \propto \exp(-2\delta d\sqrt{2m\phi}/\hbar)$, where ϕ is the work function of Au approximated as 5.0 eV and m is the electron mass. At base temperature (4.2 K), sample is repeatedly opened and closed to form atomically sharp Au electrodes, and this method allows to form molecular junctions at low temperature.⁵² Electronic transport measurements were carried out using a Yokogawa 7651 as a DC voltage source. The wiring is composed of homemade coaxial cables and SMA connectors. Current and voltage across the sample are recorded using Femto DLCPA and Femto DLPVA low noise amplifiers and measured with the help of Agilent 34410A multimeters. dl/dV measurements were carried out using HF2LI Zurich Instruments lock-in amplifiers by applying an AC modulation voltage of 0.1 mV at 317 Hz. Magnetotransport measurements were performed with an applied magnetic field up to ±10 T perpendicular to the sample plane produced from a superconducting magnet inside the liquid-He dewar. All measurements and devices were remotely controlled using a custom Python program. Control experiments utilizing helium exchange gas for thermalization confirmed that eddy-current heating effects were negligible in our experiments.

Theoretical methods Singlet-triplet model

We model the singlet-triplet Kondo effect by the Anderson impurity model side-coupled to a second S=1/2 quantum dot via an antiferromagnetic exchange interaction of strength J. The Hamiltonian is given by

$$H = H_{dot} + H_{leads} + H_{tunneling} + H_{J} + H_{B}$$
. (Equation 2)

The first term, $H_{\rm dot} = \sum_{\sigma} \varepsilon_0 d_{\sigma}^{\dagger} d_{\sigma} + U n_{d\uparrow} n_{d\downarrow}$, describes the dot Hamiltonian, representing the S = 1/2 degrees of freedom of the Blatter molecule, where ϵ_{0} is the level energy, measured relative to the Fermi level $E_{\rm F},\,n_{{
m d}\sigma}$ is the occupation number for spin $\sigma = \uparrow, \downarrow$ electrons on the dot, and *U* is the local Coulomb repulsion on the dot. The second term describes the Hamiltonian of the leads and is given by $H_{\rm leads} = \sum_{k\alpha\sigma} \epsilon_k c_{k\alpha\sigma}^\dagger c_{k\alpha\sigma}$, where $\alpha = L$, R labels the two leads and ϵ_k is the kinetic energy of the lead electrons. The third term, $H_{tunneling}$ = $\sum_{k\alpha\sigma}t_{\alpha}(c_{k\alpha\sigma}^{\dagger}d_{\sigma}+H.c.)$, describes the tunneling of electrons from the leads onto and off the dot with tunneling amplitudes t_{α} and tunneling rates $\Gamma_{\alpha} = \pi \rho_{\rm F} t_{\alpha}^2$, with $\rho_{\rm F}$ the lead electron density of states at the Fermi level. The term $H_J = J\mathbf{s}_d \cdot \mathbf{S}$ describes an antiferromagnetic (J > 0) coupling between the spin \mathbf{s}_d of the Blatter molecule and the spin \mathbf{S} of the sidecoupled quantum dot. Finally, $H_B = -g\mu_B B S_z^{tot}$ describes a magnetic field acting on the combined spin of the quantum dot and side-coupled quantum dot via the total z-component $S_z^{\rm tot} = s_{z,d} + S_z$. The above is a minimal model for the singlet-triplet Kondo effect. ^{51,53} We have generalized it to include the effects of spin-orbit coupling via an anisotropic spin exchange $J\mathbf{s}_d \cdot \mathbf{S} \rightarrow \frac{J_+}{2} (s_d^+ \mathbf{S}^- + s_d^- \mathbf{S}^+) + J_\parallel s_{d,z} s_z$ and the DM term $H_{DM} = \mathbf{D} \cdot \mathbf{s}_d \times \mathbf{S}$.

The total dot-lead tunneling rate is denoted by $\Gamma = \Gamma_L + \Gamma_R$. For a strongly correlated quantum dot, we have that $U/\Gamma \gg 1$. We shall use U/Γ = 24 for the calculations, a typical value expected for molecular junctions. For example, estimates of Γ from the experiment yielded for the Blatter molecular junction 50-60 meV. For $U/\Gamma = 24$ this implies that U = 1.2-1.4 eV, which is a reasonable value for a single-molecule device. The relevant energy scales of the above model are J and k_BT_K , where T_K is the Kondo temperature for the Anderson impurity model (obtained by setting J = D = 0 in the model). Specifically, our T_K is defined as $k_B T_K = (g\mu_B)^2/4\chi(0)$, where $\chi(0)$ is the zero-temperature spin susceptibility of the Anderson model. This $T_{\rm K}$ is close to that of the well-known Haldane expression $T_{\rm K}^{\rm H}=\sqrt{\Gamma U/2} {\rm exp}(\pi \varepsilon_0(\varepsilon_0+U)/2\Gamma U).^{54}$ See Method S3 for other definitions of Kondo scales used in the literature and their interrelationships. Calculations are presented for several values of the dimensionless ratio J/k_BT_K ranging from 1 to 100.

Numerical renormalization group method

The model (Equation 2) is diagonalized to obtain its many-body eigenstates and eigenvalues via the numerical renormalization group method.55 Briefly stated, this approach consists of three steps: (1) the conduction electron kinetic energy of the leads $\sum_{k\alpha\sigma}\epsilon_k c_{k\alpha\sigma}^{\dagger}c_{k\alpha\sigma}$ is logarithmically discretized about the Fermi level $E_{\rm F}$, taken as zero of energy, $\epsilon_k \rightarrow \epsilon_{k_n} = \pm D\Lambda^{-n}, n = 0,1,...$, with D the half-bandwidth of the leads and $\Lambda > 1$ the logarithmic discretization parameter, (2) the discretized leads are then transformed to a (tridiagonal) linear chain form using a Lanczos procedure, and (3) the resulting linear chain form of (2) is iteratively diagonalized on successively lower energy scales to obtain the eigenvalues $E_{p=1,2,...}^n$ and eigenstates $|p\rangle_n$ on all energy scales $\xi_n = D\Lambda^{-n/2}$, n = 0,1,... Knowledge of the eigenstates and eigenvalues on all energy scales then allows physical properties such as thermodynamics and Green functions to be calculated. Within this approach, with refinements described in Method S2, we calculate the magnetic field, bias voltage, and temperature dependence of the differential conductance G(V, T, B) = dI/dV via

$$G(V,T,B) = \int_{-\infty}^{+\infty} -\frac{\partial f(E - eV,T)}{\partial E} A(E,T,B)dE,$$
 (Equation 3)

where f is the Fermi function and A(E, T, B) is the spectral function of the impurity level. The general dependence of the spectral function and differential conductance on field, temperature, and energy E = eV is shown in Figures S6–S8. From G(V, T, B), we extract the magnetoresistance (MR) value at bias voltage V and temperature T via

$$MR[\%] = 100 \times (R(B) - R(0))/R(0),$$
 (Equation 4)





= $100 \times (G(V, T, B = 0) - G(V, T, B))/G(V, T, B)$. (Equation 5)

First-principle calculations

All molecular structures were optimized using Kohn-Sham density functional theory (KS-DFT) as implemented in the program package Turbomole 6.6. The B3LYP $^{57-60}$ exchange-correlation functional was used, along with Ahlrichs' def2-TZVP 61 single-particle atom-centered basis set, and Grimme's empirical dispersion corrections (DFT-D3) 62 with Becke-Johnson damping. Convergence criteria of 10^{-7} a.u. for the energy in the self-consistent-field (SCF) algorithm and 10^{-4} for the gradient in the molecular structure optimizations were applied, in combination with m4 integration grids. The coupling constants J are obtained using the Yamaguchi formula 64,65 based on the energy difference between an open-shell singlet and open-shell triplet (broken-symmetry) determinant. 66

The conductance of the junctions was evaluated assuming coherent tunneling as the dominant transport mechanism (Landauer regime). The transmissions are modeled via a Green's function approach combined with DFT calculations for zerobias electronic structures, employing the wide-band limit for the self-energies of the electrodes, as described, e.g., in Caroli et al., 67 Herrmann et al. 6,68,69 A local density of states (LDOS) of 0.036 eV⁻¹ was used. Transmission functions were evaluated with Artaios, 70 using the Fock and overlap matrices from the KS-DFT electronic structure calculations on the molecular junctions. The value of the Fermi energy is not straightforward to predict in first-principle calculations on molecular junctions, as it will be affected by factors such as the irregular atomistic shapes of the electrodes and the adsorption of non-bridging molecules on the electrodes. We therefore evaluate zero-bias conductance for a range of reasonable Fermi energies (-5, -4.5, and -4 eV)and check whether our conclusions are robust with respect to this choice. For further information please refer to the supplemental information.

RESOURCE AVAILABILITY

Lead contact

Requests for further information and resources should be directed to and will be fulfilled by the lead contact, Elke Scheer (elke.scheer@uni-konstanz.de).

Materials availability

This study did not generate new, unique materials.

Data and code availability

The experimental datasets generated during this study are available from the lead contact upon reasonable request. Raw data for all first-principle calculations can be found at https://nomad-lab.eu (https://doi.org/10.17172/NOMAD/2024.12.18-1). In this dataset, the following calculations are included: isolated monomer structure optimization (entry id: 4s6DBVjmeqvVL8pC-feW2dk2gbA_Q), monomer junction structure optimization and charge transport calculation (entry id: 6F6F8qZxeF T6etC7p3oHcZY6y7A3), dimer junctions structure optimization and charge transport (Tables S5, S7, and S8—dataset "dimer-junction-optimized-transport"), isolated dimer structure optimizations (Figure S12; Table S3—dataset "dimer-isolated-optimizations"), and dimer junctions single point calculations (dataset "dimer-junction-single-point").

ACKNOWLEDGMENTS

We thank the staff of the nano lab at the University of Konstanz for technical support. G.M. and E.S. acknowledge funding by the Deutsche Forschungsgemeinschaft (DFG) through the Collaborative Research Center SFB 767 "Controlled Nanosystems" (funding ID 32152442). K.S. and C.H. acknowledge funding via the Graduate School 2536 "nanohybrid" of the Deutsche Forschungsgemeinschaft (DFG), funding ID 408076438. M.D. and C.H. acknowledge support by the Cluster of Excellence "CUI: Advanced Imaging of Matter" of the Deutsche Forschungsgemeinschaft (DFG) (EXC 2056, funding ID 390715994). T.A.C. gratefully acknowledges computing time on the supercomputer JURECA at Forschungszentrum Jülich under grant no. JIFF23.

AUTHOR CONTRIBUTIONS

G.M. and J.Z. conducted the experiments. K.S., M.D., and T.A.C. performed the calculations. J.Z.L. and L.M.C. provided the molecules. E.S. conceived the project. All authors discussed the results. G.M., T.A.C., M.D., C.H., L.M.C., and E.S. wrote the paper with input from all authors.

DECLARATION OF INTERESTS

The authors declare no competing interests.

SUPPLEMENTAL INFORMATION

Supplemental information can be found online at https://doi.org/10.1016/j.chempr.2025.102500.

Received: September 6, 2024 Revised: January 24, 2025 Accepted: March 4, 2025 Published: March 27, 2025

REFERENCES

- Ji, L., Shi, J., Wei, J., Yu, T., and Huang, W. (2020). Air-Stable Organic Radicals: New-Generation Materials for Flexible Electronics? Adv. Mater. 32, e1908015. https://doi.org/10.1002/adma.201908015.
- Deumal, M., Vela, S., Fumanal, M., Ribas-Arino, J., and Novoa, J.J. (2021). Insights into the magnetism and phase transitions of organic radical-based materials. J. Mater. Chem. C 9, 10624–10646. https://doi.org/10.1039/D1TC01376A
- Ratera, I., and Veciana, J. (2012). Playing with Organic Radicals as Building Blocks for Functional Molecular Materials. Chem. Soc. Rev. 41, 303–349. https://doi.org/10.1039/C1CS15165G.
- Yang, C., Chen, Z., Yu, C., Cao, J., Ke, G., Zhu, W., Liang, W., Huang, J., Cai, W., Saha, C., et al. (2024). Regulation of quantum spin conversions in a single molecular radical. Nat. Nanotechnol. 19, 978–985. https://doi.org/ 10.1038/s41565-024-01632-2
- Sanvito, S. (2011). Molecular Spintronics. Chem. Soc. Rev. 40, 3336–3355. https://doi.org/10.1039/c1cs15047b.
- Herrmann, C., Solomon, G.C., and Ratner, M.A. (2010). Organic Radicals As Spin Filters. J. Am. Chem. Soc. 132, 3682–3684. https://doi.org/10. 1021/ja910483b.
- Shu, C., Yang, Z., and Rajca, A. (2023). From Stable Radicals to Thermally Robust High-Spin Diradicals and Triradicals. Chem. Rev. 123, 11954– 12003. https://doi.org/10.1021/acs.chemrev.3c00406.
- Tang, B., Zhao, J., Xu, J.-F., and Zhang, X. (2020). Tuning the stability of organic radicals: from covalent approaches to non-covalent approaches. Chem. Sci. 11, 1192–1204. https://doi.org/10.1039/c9sc06143f.
- Liu, J., Isshiki, H., Katoh, K., Morita, T., Breedlove, B.K., Yamashita, M., and Komeda, T. (2013). First Observation of a Kondo Resonance for a Stable Neutral Pure Organic Radical, 1,3,5-Triphenyl-6-Oxoverdazyl,





- Adsorbed on the Au(111) Surface. J. Am. Chem. Soc. *135*, 651–658. https://doi.org/10.1021/ja303510g.
- Müllegger, S., Rashidi, M., Fattinger, M., and Koch, R. (2013). Surface-Supported Hydrocarbon π Radicals Show Kondo Behavior. J. Phys. Chem. C Nanomater. Interfaces 117, 5718–5721. https://doi.org/10. 1021/jp310316b.
- Blatter, H.M., and Lukaszewski, H.A. (1968). A New Stable Free Radical. Tetrahedron Lett. 9, 2701–2705. https://doi.org/10.1016/S0040-4039(00) 89678-1.
- Miura, Y., and Yoshioka, N. (2015). π-Stacked structure of thiadiazolofused benzotriazinyl radical: crystal structure and magnetic properties. Chem. Phys. Lett. 626, 11–14. https://doi.org/10.1016/j.cplett.2015. 03.009.
- 13. Yan, B., Cramen, J., McDonald, R., and Frank, N.L. (2011). Ferromagnetic Spin-Delocalized Electron Donors for Multifunctional Materials: π -Conjugated Benzotriazinyl Radicals. Chem. Commun. (Camb) 47, 3201–3203. https://doi.org/10.1039/C0CC04727A.
- Grant, J.A., Lu, Z., Tucker, D.E., Hockin, B.M., Yufit, D.S., Fox, M.A., Kataky, R., Chechik, V., and O'Donoghue, A.C. (2017). New Blatter-type radicals from a bench-stable carbene. Nat. Commun. 8, 15088. https://doi.org/10.1038/ncomms15088.
- Ciccullo, F., Gallagher, N.M., Geladari, O., Chassé, T., Rajca, A., and Casu, M.B. (2016). A Derivative of the Blatter Radical as a Potential Metal-Free Magnet for Stable Thin Films and Interfaces. ACS Appl. Mater. Interfaces 8, 1805–1812. https://doi.org/10.1021/acsami.5b09693.
- Low, J.Z., Kladnik, G., Patera, L.L., Sokolov, S., Lovat, G., Kumarasamy, E., Repp, J., Campos, L.M., Cvetko, D., Morgante, A., et al. (2019). The Environment-Dependent Behavior of the Blatter Radical at the Metal-Molecule Interface. Nano Lett. 19, 2543–2548. https://doi.org/10.1021/ acs.nanolett.9b00275.
- Patera, L.L., Sokolov, S., Low, J.Z., Campos, L.M., Venkataraman, L., and Repp, J. (2019). Resolving the Unpaired-Electron Orbital Distribution in a Stable Organic Radical by Kondo Resonance Mapping. Angew. Chem. Int. Ed. Engl. 58, 11063–11067. https://doi.org/10.1002/anie.201904851.
- Zheng, Y., Miao, M.S., Dantelle, G., Eisenmenger, N.D., Wu, G., Yavuz, I., Chabinyc, M.L., Houk, K.N., and Wudl, F. (2015). A Solid-State Effect Responsible for an Organic Quintet State at Room Temperature and Ambient Pressure. Adv. Mater. 27, 1718–1723. https://doi.org/10.1002/adma.201405093.
- Hurtado-Gallego, J., Sangtarash, S., Davidson, R., Rincón-García, L., Daaoub, A., Rubio-Bollinger, G., Lambert, C.J., Oganesyan, V.S., Bryce, M.R., Agraït, N., et al. (2022). Thermoelectric Enhancement in Single Organic Radical Molecules. Nano Lett. 22, 948–953. https://doi.org/10. 1021/acs.nanolett.1c03698.
- Khurana, R., Bajaj, A., and Ali, M.E. (2020). How Plausible Is Getting Ferromagnetic Interactions by Coupling Blatter's Radical via Its Fused Benzene Ring?
 Phys. Chem. A 124, 6707–6713. https://doi.org/10.1021/acs.jpca.0c05719.
- Ji, Y., Long, L., and Zheng, Y. (2020). Recent Advances of Stable Blatter Radicals: Synthesis, Properties and Applications. Mater. Chem. Front. 4, 3433–3443. https://doi.org/10.1039/D0QM00122H.
- Madhavan, V., Chen, W., Jamneala, T., Crommie, M.F., and Wingreen, N.S. (1998). Tunneling into a Single Magnetic Atom: Spectroscopic Evidence of the Kondo Resonance. Science 280, 567–569. https://doi.org/10.1126/science.280.5363.567.
- Ternes, M., Heinrich, A.J., and Schneider, W.D. (2009). Spectroscopic Manifestations of the Kondo Effect on Single Adatoms. J. Phys. Condens. Matter 21, 053001. https://doi.org/10.1088/0953-8984/21/5/053001.
- Jiang, Y., Li, S., Wang, Y., Pan, H., Wang, Y., Sanvito, S., and Hou, S. (2023). Does a Blatter Radical Retain Its Open-Shell Character When Incorporated into Gold-Molecule-Gold Junctions? J. Phys. Chem. C 127, 9268–9277. https://doi.org/10.1021/acs.jpcc.3c00224.

- Frisenda, R., Gaudenzi, R., Franco, C., Mas-Torrent, M., Rovira, C., Veciana, J., Alcon, I., Bromley, S.T., Burzurí, E., and Van Der Zant, H.S.J. (2015). Kondo effect in a Neutral and Stable All Organic Radical Single Molecule Break Junction. Nano Lett. 15, 3109–3114. https://doi.org/10.1021/acs.nanolett.5b00155.
- Hayakawa, R., Karimi, M.A., Wolf, J., Huhn, T., Zöllner, M.S., Herrmann, C., and Scheer, E. (2016). Large Magnetoresistance in Single-Radical Molecular Junctions. Nano Lett. 16, 4960–4967. https://doi.org/10.1021/acs.nanolett.6b01595.
- Zhang, Y., Qiu, R., Qu, K., Zhang, C., Stoddart, J.F., and Chen, H. (2024).
 Organic radicals in single-molecule junctions. Sci. China Mater. 67, 709–728. https://doi.org/10.1007/s40843-024-2792-0.
- Kertesz, M. (2019). Pancake Bonding: an Unusual Pi-Stacking Interaction. Chemistry 25, 400–416. https://doi.org/10.1002/chem.201802385.
- Park, Y.S., Widawsky, J.R., Kamenetska, M., Steigerwald, M.L., Hybertsen, M.S., Nuckolls, C., and Venkataraman, L. (2009). Frustrated rotations in single-molecule junctions. J. Am. Chem. Soc. *131*, 10820–10821. https://doi.org/10.1021/ja903731m.
- Feng, Q., Yamada, A., Baer, R., and Dunietz, B.D. (2016). Deleterious effects of exact exchange functionals on predictions of molecular conductance.
 J. Chem. Theory Comput. 12, 3431–3435. https://doi.org/10.1021/acs.jctc.6b00493.
- Strange, M., Rostgaard, C., Häkkinen, H., and Thygesen, K.S. (2011). Self-consistent GW calculations of electronic transport in thiol- and amine-linked molecular junctions. Phys. Rev. B 83, 115108. https://doi.org/10.1103/PhysRevB.83.115108.
- Koentopp, M., Chang, C., Burke, K., and Car, R. (2008). Density functional calculations of nanoscale conductance. J. Phys.: Condens. Matter 20, 083203. https://doi.org/10.1088/0953-8984/20/8/083203.
- Ke, S.-H., Baranger, H.U., and Yang, W. (2007). Role of the exchange-correlation potential in ab initio electron transport calculations. J. Chem. Phys. 126, 201102. https://doi.org/10.1063/1.2743004.
- Frisenda, R., Janssen, V.A.E.C., Grozema, F.C., van der Zant, H.S.J., and Renaud, N. (2016). Mechanically controlled quantum interference in individual π -stacked dimers. Nat. Chem. 8, 1099–1104. https://doi.org/10. 1038/nchem.2588.
- Knaak, T., Gruber, M., Lindström, C., Bocquet, M.L., Heck, J., and Berndt, R. (2017). Ligand-Induced Energy Shift and Localization of Kondo Resonances in Cobalt-Based Complexes on Cu(111). Nano Lett. 17, 7146–7151. https://doi.org/10.1021/acs.nanolett.7b04181.
- Žitko, R. (2010). Fano-Kondo Effect in Side-Coupled Double Quantum Dots at Finite Temperatures and the Importance of Two-Stage Kondo Screening. Phys. Rev. B 81, 115316. https://doi.org/10.1103/PhysRevB. 81.115316.
- Sasaki, S., Tamura, H., Akazaki, T., and Fujisawa, T. (2009). Fano-Kondo Interplay in a Side-Coupled Double Quantum Dot. Phys. Rev. Lett. 103, 266806. https://doi.org/10.1103/PhysRevLett.103.266806.
- Rosch, A., Costi, T.A., Paaske, J., and Wölfle, P. (2003). Spectral function of the Kondo model in high magnetic fields. Phys. Rev. B 68, 014430. https://doi.org/10.1103/PhysRevB.68.014430.
- Frota, H.O., and Oliveira, L.N.D. (1986). Photoemission spectroscopy for the spin-degenerate Anderson model. Phys. Rev. B Condens. Matter 33, 7871–7874. https://doi.org/10.1103/PhysRevB.33.7871.
- Újsághy, O., Kroha, J., Szunyogh, L., and Zawadowski, A. (2000). Theory
 of the Fano resonance in the STM tunneling density of states due to a single Kondo impurity. Phys. Rev. Lett. 85, 2557–2560. https://doi.org/10.
 1103/PhysRevLett.85.2557.
- van Efferen, C., Fischer, J., Costi, T.A., Rosch, A., Michely, T., and Jolie, W. (2024). Modulated Kondo screening along magnetic mirror twin boundaries in monolayer MoS 22. Nat. Phys. 20, 82–87. https://doi.org/10.1038/s41567-023-02250-w.
- Appelt, W.H., Droghetti, A., Chioncel, L., Radonjić, M.M., Muñoz, E., Kirchner, S., Vollhardt, D., and Rungger, I. (2018). Predicting the Conductance





- of Strongly Correlated Molecules: The Kondo Effect in Perchlorotriphenyl-methyl/Au Junctions. Nanoscale *10*, 17738–17750. https://doi.org/10.1039/C8NR03991G.
- Parks, J.J., Champagne, A.R., Hutchison, G.R., Flores-Torres, S., Abruña, H.D., and Ralph, D.C. (2007). Tuning the Kondo Effect with a Mechanically Controllable Break Junction. Phys. Rev. Lett. 99, 026601. https://doi.org/ 10.1103/PhysRevLett.99.026601.
- Costi, T.A. (2000). Kondo Effect in a Magnetic Field and the Magnetoresistivity of Kondo Alloys. Phys. Rev. Lett. 85, 1504–1507. https://doi.org/10. 1103/PhysRevLett.85.1504.
- Hsu, C., Costi, T.A., Vogel, D., Wegeberg, C., Mayor, M., Van Der Zant, H.S.J., and Gehring, P. (2022). Magnetic-field universality of the Kondo effect revealed by thermocurrent spectroscopy. Phys. Rev. Lett. 128, 147701. https://doi.org/10.1103/PhysRevLett.128.147701.
- Mitra, G., Low, J.Z., Wei, S., Francisco, K.R., Deffner, M., Herrmann, C., Campos, L.M., and Scheer, E. (2022). Interplay between Magnetoresistance and Kondo Resonance in Radical Single-Molecule Junctions. Nano Lett. 22, 5773–5779. https://doi.org/10.1021/acs.nanolett.2c01199.
- Xie, Z., Shi, S., Liu, F., Smith, D.L., Ruden, P.P., and Frisbie, C.D. (2016).
 Large Magnetoresistance at Room Temperature in Organic Molecular Tunnel Junctions with Nonmagnetic Electrodes. ACS Nano 10, 8571– 8577. https://doi.org/10.1021/acsnano.6b03853.
- Shi, S., Xie, Z., Liu, F., Smith, D.L., Frisbie, C.D., and Ruden, P.P. (2017). Theory of Magnetoresistance of Organic Molecular Tunnel Junctions with Nonmagnetic Electrodes. Phys. Rev. B 95, 155315. https://doi.org/ 10.1103/PhysRevB.95.155315.
- Parks, J.J., Champagne, A.R., Costi, T.A., Shum, W.W., Pasupathy, A.N., Neuscamman, E., Flores-Torres, S., Cornaglia, P.S., Aligia, A.A., Balseiro, C.A., et al. (2010). Mechanical control of spin states in spin-1 molecules and the underscreened Kondo effect. Science 328, 1370–1373. https:// doi.org/10.1126/science.1186874.
- Zalom, P., De Bruijckere, J., Gaudenzi, R., Van Der Zant, H.S.J., Novotný, T.K.R.M., and Korytár, R. (2019). Magnetically Tuned Kondo effect in a molecular double quantum dot: role of the anisotropic exchange. J. Phys. Chem. C 123, 11917–11925. https://doi.org/10.1021/acs.jpcc. 9b00783
- Pustilnik, M., and Glazman, L.I. (2000). Conduction through a quantum dot near a singlet-triplet transition. Phys. Rev. Lett. 85, 2993–2996. https://doi. org/10.1103/PhysRevLett.85.2993.
- Reichert, J., Weber, H.B., Mayor, M., and v Löhneysen, H. (2003). Low-Temperature Conductance Measurements on Single Molecules. Appl. Phys. Lett. 82. 4137–4139. https://doi.org/10.1063/1.1574844.
- Paaske, J., Rosch, A., Wölfle, P., Mason, N., Marcus, C.M., and Nygård, J. (2006). Non-equilibrium singlet-triplet Kondo effect in carbon nanotubes. Nat. Phys. 2, 460–464. https://doi.org/10.1038/nphys340.
- 54. Hewson, A.C. (1997). The Kondo Problem to Heavy Fermions, Second Edition (Cambridge University Press).
- Wilson, K.G. (1975). The renormalization group: critical phenomena and the Kondo problem. Rev. Mod. Phys. 47, 773–840. https://doi.org/10. 1103/RevModPhys.47.773.
- Balasubramani, S.G., Chen, G.P., Coriani, S., Diedenhofen, M., Frank, M.S., Franzke, Y.J., Furche, F., Grotjahn, R., Harding, M.E., Hättig, C., et al. (2020). TURBOMOLE: modular program suite for ab initio quan-

- tum-chemical and condensed-matter simulations. J. Chem. Phys. 152, 184107. https://doi.org/10.1063/5.0004635.
- Becke, A.D. (1993). Density-functional thermochemistry. III. the role of exact exchange. J. Chem. Phys. 98, 5648–5652. https://doi.org/10. 1063/1.464913.
- Lee, C., Yang, W., and Parr, R.G. (1988). Development of the Colle-Salvetti correlation-energy formula into a functional of the electron density. Phys. Rev. B Condens. Matter 37, 785–789. https://doi.org/10.1103/physrevb. 37.785.
- Vosko, S.H., Wilk, L., and Nusair, M. (1980). Accurate spin-dependent electron liquid correlation energies for local spin density calculations: a critical analysis. Can. J. Phys. 58, 1200–1211. https://doi.org/10.1139/ p80-159.
- Stephens, P.J., Devlin, F.J., Chabalowski, C.F., and Frisch, M.J. (1994). Ab initio calculation of vibrational absorption and circular dichroism spectra using density functional force fields. J. Phys. Chem. 98, 11623–11627. https://doi.org/10.1021/j100096a001.
- Weigend, F., and Ahlrichs, R. (2005). Balanced basis sets of split valence, triple zeta valence and quadruple zeta valence quality for H to Rn: design and assessment of accuracy. Phys. Chem. Chem. Phys. 7, 3297–3305. https://doi.org/10.1039/B508541A.
- Grimme, S., Antony, J., Ehrlich, S., and Krieg, H. (2010). A consistent and accurate ab initio parametrization of density functional dispersion correction (DFT-D) for the 94 elements H-Pu. J. Chem. Phys. 132, 154104. https://doi.org/10.1063/1.3382344.
- Grimme, S., Ehrlich, S., and Goerigk, L. (2011). Effect of the damping function in dispersion corrected density functional theory. J. Comput. Chem. 32, 1456–1465. https://doi.org/10.1002/jcc.21759.
- Kitagawa, Y., Saito, T., and Yamaguchi, K. (2018). Chapter 7: Approximate spin projection for broken-symmetry method and its application. In Symmetry (Group Theory) and Mathematical Treatment in Chemistry, T. Akitsu, ed. (IntechOpen). https://doi.org/10.5772/intechopen.75726.
- Yamanaka, S., Takeda, R., Shoji, M., Kitagawa, Y., Honda, H., and Yama-guchi, K. (2005). Quantum spin correction scheme for ab initio spin-unrestricted solutions: multiple bonds case. Int. J. Quantum Chem. 105, 605–614. https://doi.org/10.1002/qua.20738.
- Noodleman, L. (1981). Valence bond description of antiferromagnetic coupling in transition metal dimers. J. Chem. Phys. 74, 5737–5743. https://doi.org/10.1063/1.440939.
- Caroli, C., Combescot, R., Nozieres, P., and Saint-James, D. (1971). Direct calculation of the tunneling current. J. Phys. C: Solid State Phys. 4, 916–929. https://doi.org/10.1088/0022-3719/4/8/018.
- Herrmann, C., Solomon, G.C., Subotnik, J.E., Mujica, V., and Ratner, M.A. (2010). Ghost transmission: how large basis sets can make electron transport calculations worse. J. Chem. Phys. 132, 24103. https://doi.org/10.1063/1.3283062.
- Herrmann, C., Solomon, G.C., and Ratner, M.A. (2011). Designing organic spin filters in the coherent tunneling regime. J. Chem. Phys. 134, 0224306. https://doi.org/10.1063/1.3598519.
- Deffner, M., Groß, L., Steenbock, T., Voigt, B.A., Zöllner, M.S., Solomon, G.C., and Herrmann, C. (2008–2024). A postprocessing framework for electronic structure calculations. https://www.chemie.uni-hamburg.de/ institute/ac/arbeitsgruppen/herrmann/software/artaios.html.